Ceramics International xxx (xxxx) xxx–xxx

Contents lists available at ScienceDirect

Ceramics International

journal homepage: www.elsevier.com/locate/ceramint

Evaluation of mechanical properties of Al_2O_3–Cr_2O_3 ceramic system prepared in different Cr_2O_3 ratios for ceramic armour components

Betül Kafkaslıoğlu Yıldız*, Hüseyin Yılmaz, Yahya Kemal Tür

Department of Materials Science and Engineering, Gebze Technical University, Gebze, Turkey

ARTICLE INFO

Keywords:
Al_2O_3
Cr_2O_3
Armour
Mechanical properties

ABSTRACT

The aim of the present study was to introduce Al_2O_3–Cr_2O_3 ceramic system as an armour material by evaluating its performance with static mechanical tests. Cr_2O_3 was used as an additive to the pure Al_2O_3 owing to the character of substitutional solid solution formation that would provide increases in mechanical properties. The effect of Cr_2O_3 addition in different volume ratios (0.5, 1, 5 vol%) on the microstructure and the mechanical properties (elastic modulus, equibiaxial flexural strength, hardness, fracture toughness) of Al_2O_3 were investigated. Densification behavior and grain size of Al_2O_3 changed with the amount of Cr_2O_3, the highest relative density and grain size were obtained for 1 vol% Cr_2O_3 added Al_2O_3–Cr_2O_3 system. A 44% increase in flexural strength was achieved by 0.5 vol% Cr_2O_3 addition and attributed to the localized compressive stresses because of the grain boundary modification of the larger size of the Cr^{3+} ions. 1 vol % Cr_2O_3 addition increased the hardness 13% while the effect of Cr_2O_3 on toughness was negligible. The fragmentation behavior was discussed as a function of the stored energy at failure and total crack surface area. A shorter crack length for a given stored energy was observed for 0.5 vol% Cr_2O_3 composition compared to other compositions indicating its fragments would be larger in identical impact conditions increasing the erosion of the projectile.

1. Introduction

Alumina (Al_2O_3) based ceramics have been widely used for structural applications including armour components as a result of their attractive thermal, chemical and mechanical properties [1–3]. However, Al_2O_3 ceramics have some disadvantages compared with the other monolithic carbide ceramics (i.e. SiC and B_4C) especially when they are used in armour applications [4,5]. Al_2O_3 possesses high density (3.98 g/cm^3) and its flexural strength and hardness are lower than the most carbide ceramics [4,6]. Incorporation of second phase particles which include ZrO_2, SiC, B_4C, TiC, Cr_3C_2 into Al_2O_3 increases its mechanical properties but sintering the carbide containing ceramics needs high temperatures or costly techniques such as hot pressing [7–9]. ZrO_2 addition to Al_2O_3 (ZTA) increases the density of the material with its relatively high density (6.10 g/cm^3) and generally decreases the hardness of Al_2O_3 [10].

In addition to second phase particles, solid solution formation can be considered as an alternative for improving the mechanical properties for Al_2O_3 ceramics in armour applications. Chromia (Cr_2O_3) and Al_2O_3 have isostructural corundum crystal structure (hexagonal system of same space group R–3c) and it is well known that Cr_2O_3 forms a substitutional solid solution in Al_2O_3 lattice by exchange with Al^{3+} ions over the full range of compositions (T > 1000 °C) without formation of any eutectic [2,11,12]. There are several studies that Cr_2O_3 is added to Al_2O_3 in different ratios with different consolidation techniques to increase the mechanical properties of the ceramic [13–16]. It is stated that isovalent solid solution formation provides high refractoriness and chemical stability to the ceramic [13,14]. Also, the toughness, tensile strength, and hardness of Al_2O_3 were increased with the addition of Cr_2O_3 in a number of studies caused by the changes in the microstructure [15,16]. Riu et al. [16] reported a decrease in strength but an increase in toughness due to the crack bridging of the large plate-like grains with ~2 mol% (2.26 vol%) Cr_2O_3 addition; they also observed an increase in the elastic modulus and the hardness. Azhar et al. [2] fabricated the Al_2O_3–ZrO_2–Cr_2O_3 system with different Cr_2O_3 ratios ranging from 0 to 1 wt% (0.76 vol%) to increase the mechanical properties of ZrO_2 toughened Al_2O_3 composites in wear applications. An addition of 0.6 wt% (0.46 vol%) of Cr_2O_3 resulted in minimum wear area accompanied with 2.6% and 7% increase in hardness and toughness, respectively. However, Kuntz and Krüger [17] investigated the Al_2O_3–ZrO_2–Cr_2O_3 system and reported that there is no effect of Cr_2O_3 addition to the mechanical performance up to the amount of 0.5 wt% (0.38 vol%).

Developing and evaluating the performance of multi-phase ceramics

* Corresponding author.
E-mail address: bkafkaslioglu@gtu.edu.tr (B. Kafkaslıoğlu Yıldız).

https://doi.org/10.1016/j.ceramint.2019.07.037
Received 13 May 2019; Received in revised form 17 June 2019; Accepted 3 July 2019

and novel composites with relatively low cost of processing and equipment for armour applications is required in order to overcome the shortcomings of monolithic ceramics [18]. Although there are many studies about the mechanical properties of Al_2O_3–Cr_2O_3 system in the literature, a detailed study that analyzes the mechanical properties to evaluate the material system as an armour component is not available. In the present work, we investigated the effect Cr_2O_3 addition in different volume ratios (0.5, 1, 5 vol%) on microstructure and mechanical properties of Al_2O_3 (elastic modulus, equibiaxial flexural strength, toughness, and hardness) for use in armour applications. The Cr_2O_3 content was selected according to the literature summarized above and the preliminary studies with small-sized pellets (13 mm diameter) for different Cr_2O_3 volume ratios. Cr_2O_3 has a higher density (5.22 g/cm^3) than Al_2O_3 and increasing the specific density in armour applications is not desired; therefore, the maximum Cr_2O_3 content was kept at 5 vol%. The equibiaxial flexural test that provides large fracture surface area and fracture pattern similar to ballistically tested material was used to measure the strength of the ceramics and to evaluate the fragmentation behavior [19,20].

The densification character of the Al_2O_3–Cr_2O_3 ceramic system depends on the sintering temperature, atmosphere, and the Cr_2O_3 content. Cr_2O_3 is not stable in an atmosphere with high oxygen partial pressure and evaporation of gaseous species such as CrO_3 occurs above 1000°C [12,21]. Therefore, sintering of Al_2O_3–Cr_2O_3 ceramic is generally performed under reducing or inert atmosphere [22,23]. In this work, the prepared powders were pressureless sintered at 1550°C in 90%Ar/10% H_2 to reduce the volatilization. Low Cr_2O_3 contents (< 5 mol% (5.74 vol%)) requires lower sintering temperatures than high contents for densification [21]. For ceramic armour materials, increasing the sintering temperature can be a disadvantage because selecting high sintering temperatures would diminish Al_2O_3 based ceramics/composites' cost benefit. The sintering temperature was determined according to the preliminary studies that were carried out for the pure Al_2O_3 and the present literature about the Al_2O_3–Cr_2O_3 ceramic system. Nath et al. [12] stated in their work that apparent porosity drops down to zero for Al_2O_3–Cr_2O_3 samples that were pressureless sintered at 1550°C in reducing atmosphere. Xia et al. [24] pressureless sintered their ZTA samples containing different amounts of Cr_2O_3 (0.08, 0.2, 0.5, 0.8 wt%) at 1540°C/2 h in air.

2. Experimental procedure

Al_2O_3 powder (Alfa Aesar, α-Al_2O_3, 99.95% purity, 0.25–0.45 μm), Cr_2O_3 powder (Alfa Aesar, 99% metals basis, mean particle size ~200 nm), polyacrylic acid as dispersant (Darvan 821A, MSE Technology Co. Ltd., Turkey) and polypropylene carbonate (PPC) (QPAC 40, Empower Materials, USA) as binder were used in this study. α-Al_2O_3 powder, different ratios of Cr_2O_3 additive (0.5, 1, 5 vol%) and 0.5 wt% dispersant were firstly mixed in distilled water and ball milled for 24 h with Al_2O_3 balls. Subsequently, the mixture was dried in hotplate at 80°C. A heat treatment at 500°C/2 h in air was carried out for the Al_2O_3–Cr_2O_3 powder mixtures to eliminate the dispersant. 3 wt% PPC was added to the powder mixtures from the prepared stock solution with acetone solvent and the acetone was evaporated while stirring under fume cupboard. The powder mixtures were crushed and passed through 90 μm sieve then uniaxially pressed under 40 MPa by using a 35 mm diameter steel mold. Then, cold isostatic pressing was performed under 200 MPa pressure and the green density in the range of 56–60% was obtained for all the ceramics. The specimens were pressureless sintered at 1550°C for 2 h in 90%Ar/10%H_2 atmosphere with 5°C min^{-1} heating rate after burning out the binder at about 350°C and furnace cooled. The dimensions of the sintered specimens were around 29 mm in diameter and 2.5 mm in thickness after the sintering. Pure Al_2O_3 specimens were prepared under the same conditions and sintered in air with the same heating regime.

All the specimens were grinded by a single-sided lapping machine with an average particle size of 30 μm SiC powder (F320) and 1200 grade SiC abrasive paper to equalize thickness of the pellets (with ± 0.03 tolerance) for the mechanical property measurements. The bulk density of the sintered specimens was calculated with the direct measurements of mass and macroscopic dimensions instead of Archimedes' method because of the lower standard deviations and better repeatability. Determining the theoretical density for solid solutions is one of the primary areas of research [13]. Nevertheless, in this study, theoretical densities of the ceramics were calculated by the rule of mixtures to estimate the relative densities from the theoretical densities of Al_2O_3 and Cr_2O_3 to compare its densification behavior with the pure Al_2O_3.

The crystalline structure and phase composition of the specimens were identified by X-ray diffraction method by a Bruker® D8 Advance diffractometer at a scanning rate of 3°/min from 20° to 70° and 0.1°/min from 34° to 36° to examine the diffraction peak of the (104) crystal face that is the sharpest and has the highest intensity. Elastic modulus was measured using an impulse excitation technique (GrindoSonic® Mk5) in accordance with ASTM E 1876-01 standard with disc-shaped samples. The theoretical value of the elastic modulus of the Al_2O_3–Cr_2O_3 system was calculated by averaging the Voigt (Rule of mixtures) and Reuss (Inverse rule of mixtures) bounds for the materials, known as VRH average [25]. SiC powder (F600) with an average particle size of 9 μm and diamond suspension of 1 μm was used for polishing before etching; the microstructural analysis was performed by scanning electron microscopy (SEM) (Philips XL 30 SFEG). The specimens were thermally etched in the same furnace used for sintering at 1400 °C/2 h in H_2/Ar atmosphere for the Al_2O_3–Cr_2O_3 ceramics and in air for the pure Al_2O_3. The grain size of the Al_2O_3–Cr_2O_3 ceramic systems was measured with the linear intercept method where more than 100 intercepts were counted.

The Vickers indentation technique was conducted with an Instron® Wolpert Testor 2100 to measure the hardness and toughness of the specimens with a load of 5 kg for the hardness with thirty measurements from different specimens in each content and 20 kg for the toughness. The fracture toughness was calculated with the equation given by Anstis [26] using the crack length measurements from five indentations for each composition; the crack lengths were measured by using SEM for high accuracy. Monotonic equibiaxial flexural test (ring on ring) was used to measure the strength of the specimens and conducted with an Instron® 5569 universal test device according to ASTM C 1499–03 after grinding and polishing under the same conditions. The displacement rate was set at 0.3 mm/min and the diameter of the support ring and the load ring was 23.9 mm and 9.8 mm, respectively. Ten specimens of each ceramic were used for the strength measurements and a lubricant was applied to the ring tips to eliminate frictional stresses. The equation for the equibiaxial strength (σ_f *(MPa)*) of a circular sample:

$$\sigma_f = \frac{3F}{2\pi h^2}\left[(1-\nu)\frac{D_s^2 - D_L^2}{2D^2} + (1+\nu)\ln\frac{D_s}{D_L}\right] \quad (1)$$

where F is the breaking load (N), D is the diameter (mm), h is the thickness (mm), ν is Poisson's ratio, D_S is the support ring diameter (mm), and D_L is the load ring diameter (mm). After the tests, photographs were taken of all the samples and the total crack lengths were measured using an image analysis software. The total crack area is evaluated by multiplying the measured crack length with the specimen thickness for each specimen.

3. Results and discussion

XRD patterns of the sintered ceramics with different content of Cr_2O_3 were presented in Fig. 1. Al_2O_3 and Cr_2O_3 have the same corundum crystal structure; in the XRD analysis, only the corundum peaks were identified as expected and no new compound was found with the addition of Cr_2O_3. It is stated in the literature that the lattice parameters

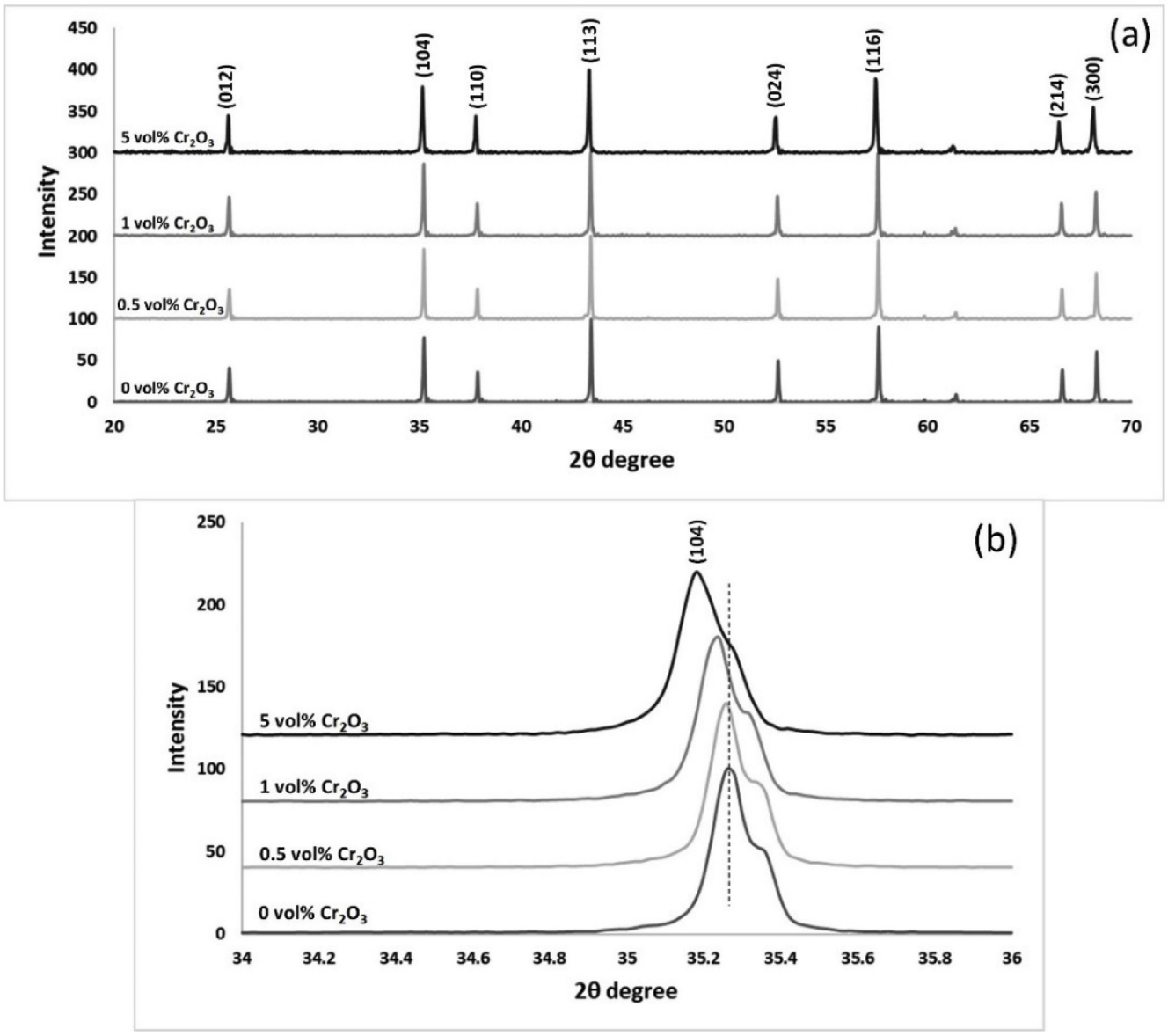

Fig. 1. a) XRD patterns of the sintered ceramics with different content of Cr_2O_3, and b) XRD was zoomed in from 34° to 36° to show the shifting of the (104) peak with the increasing Cr_2O_3 content. The vertical dashed line marks the peak of the pure Al_2O_3.

of the corundum structure "a" and "c" increases linearly with the Cr_2O_3 content as in agreement with Vegard's law. As the radii of Cr^{3+} ion (0.076 nm) is bigger than Al^{3+} ion (0.068 nm), the dissolution of Cr_2O_3 increases the Al_2O_3 lattice dimensions so the angle of diffraction peaks decreases according to Bragg's law [13,24]. The angle of XRD was zoomed in from 34° to 36° as shown in Fig. 1(b) to verify the increase in the Cr_2O_3 content since the amount of Cr_2O_3 in the solid solution could be determined based on the high intensity (104) diffraction peak [13]. Fig. 1(b) shows the shifting of the (104) peak to the lower angles with the increase in the Cr_2O_3 content, especially for 5 vol%.

Table 1 shows the measured physical and mechanical properties of the Al_2O_3–Cr_2O_3 ceramics for 0.5 vol%, 1 vol% and 5 vol% Cr_2O_3 contents and the pure Al_2O_3 (referred as 0.5CR, 1CR, 5CR, and A, respectively). Al_2O_3 powder used in this research was not doped with any sintering aid (i.e. MgO) and showed poor densification with 95.7% relative density. Cr_2O_3 is prone to vaporization even at very low oxygen partial pressures and the evaporation-condensation mechanism of Cr_2O_3 inhibits obtaining the fully dense pure Cr_2O_3. Also, the formation

Table 1
The measured physical and mechanical properties of the Al_2O_3–Cr_2O_3 ceramics for all the Cr_2O_3 contents.

Composition	Relative Density (%)	Alumina Grain Size (μm)	Elastic Modulus (GPa)	Relative Elastic Modulus (%)	Flexural Strength (MPa)	Total Crack Area (mm^2)	Fracture Toughness ($MPa\sqrt{m}$)	Hardness (GPa)
A	95.7	~0.85	362 ± 6	90.5	199 ± 53	113 ± 53	3.73 ± 0.16	20.2 ± 1.1
0.5CR	95.8	~1.31	364 ± 10	91.2	286 ± 47	231 ± 66	3.84 ± 0.35	21.4 ± 1.6
1CR	96.7	~1.42	373 ± 4	93.6	237 ± 47	187 ± 65	3.81 ± 0.19	22.8 ± 1.3
5CR	93.8	~1.30	341 ± 11	86.8	221 ± 50	173 ± 71	3.84 ± 0.35	19.0 ± 2.0

of solid solution absorbs extra heat energy that results in ceramics with low densities [11]. On the other hand, it is stated that solid solution formation enhances the mass transportation which results in high densification [27], and these results are valid for the Al_2O_3–Cr_2O_3 system to some extent. The solid-state solution is one of the driving forces contributing the total mass transport. Bueno et al. [28] explained the densification mechanism for SnO_2–TiO_2 binary composition. The evaporation-condensation mechanism decreases (for SnO_2 in their study and Cr_2O_3 in the present study) and mass transport through the boundary may take place. 0.5 vol% Cr_2O_3 addition had no considerable effect on the densification and the same relative density was obtained with the pure Al_2O_3. The highest densification was achieved for 1 vol% Cr_2O_3 addition and it was attributed to sufficient solid solution formation supporting densification without significant vaporization. 5 vol % Cr_2O_3 addition to Al_2O_3 prevented the densification because of the expected evaporation behavior of Cr_2O_3 while sintering [11,22]. These observations can also be quantified by percent porosity: the porosity of A and 0.5CR samples were 4.3 and 4.2%, it decreased to 3.3% for 1CR samples and increased to 6.2% for 5CR samples.

The relative elastic modulus of the ceramics was calculated by the ratio of the measured elastic modulus to the VRH average; in VHR average calculations the elastic modulus of Al_2O_3 and Cr_2O_3 were 400 and 280 GPa, respectively [29,30]. The relative elastic modulus values increased with the densification correspondingly and the highest elastic modulus was obtained for 1 vol% Cr_2O_3 addition as seen in Table 1. The importance of densification in obtaining high mechanical properties of ceramic materials is evident; higher the relative density, higher the elastic modulus values.

SEM micrographs of polished and thermally etched ceramics without and with different content of Cr_2O_3 additives are presented in Fig. 2. The dark grains represent the corundum phase and because of the solid solution formation, Cr_2O_3 grains could not be recognized as distinct from the Al_2O_3 grains. Also, the Al_2O_3 grain sizes measured by using the linear intercept method are given in Table 1. Al_2O_3 grain growth occurred with the addition of Cr_2O_3 for all the ratios, especially in 1 vol%. As the solid solution proceeds, the presence of Cr^{3+} ions induces an increase in the growth rate of Al_2O_3 because of the coherency strain energy at the grain boundary. At a temperature that is high enough for the grain boundary mobility, generally, a chemically induced boundary migration happens in solid solutions [31]. Rapid migration of grain boundaries as a result of coherency strain energy causes changes in the microstructure [16]. The highest grain size was measured for 1CR in parallel to its highest relative density. However, the Al_2O_3 grain sizes differed from region to region significantly for both pure Al_2O_3 and the other ceramics with different content of Cr_2O_3 additives because of the lack of sintering aid and relatively low densification.

The equibiaxial flexural strength values given in Table 1 shows that the pure Al_2O_3 has a strength of 199 MPa, a relatively low strength. This low strength can be attributed to low densification of the pure Al_2O_3, in other words, larger defect size. 0.5 vol% Cr_2O_3 addition dramatically increased the flexural strength value to 286 MPa even though they have the same relative density. Li et al. [15] also observed an increase in flexural strength of Al_2O_3 with 0.4 mol% Cr_2O_3 (0.46 vol%) addition and argued that grain boundary modification caused by the larger size of the Cr^{3+} ions replacing Al^{3+} ions results in localized compressive stresses and increased the fracture strength. This compressive stresses would contribute to the strengthening of the material because the penetration of the crack through the grain boundary is hindered. The ion size misfit would provide the mechanism for the 43% increase in strength in 0.5CR ceramics. Localized compressive stresses due to ion size misfit start to overlap with increasing Cr_2O_3 content and its effect diminishes [15]. Consequently, the strength of 1CR and 5CR ceramics are lower than 0.5CR, yet higher than the pure Al_2O_3.

For ceramic materials, deformation is elastic; therefore, the stored elastic energy is equal to the work done by the force on a specimen and it can be evaluated by the area below the load-displacement (P-Δ) curve. For ceramic materials, the load-displacement relationship is linear so the stored elastic energy (U) can be calculated with the equation:

$$U = \frac{1}{2} P\Delta \tag{2}$$

where P is the applied load (N) and Δ is the displacement of the load

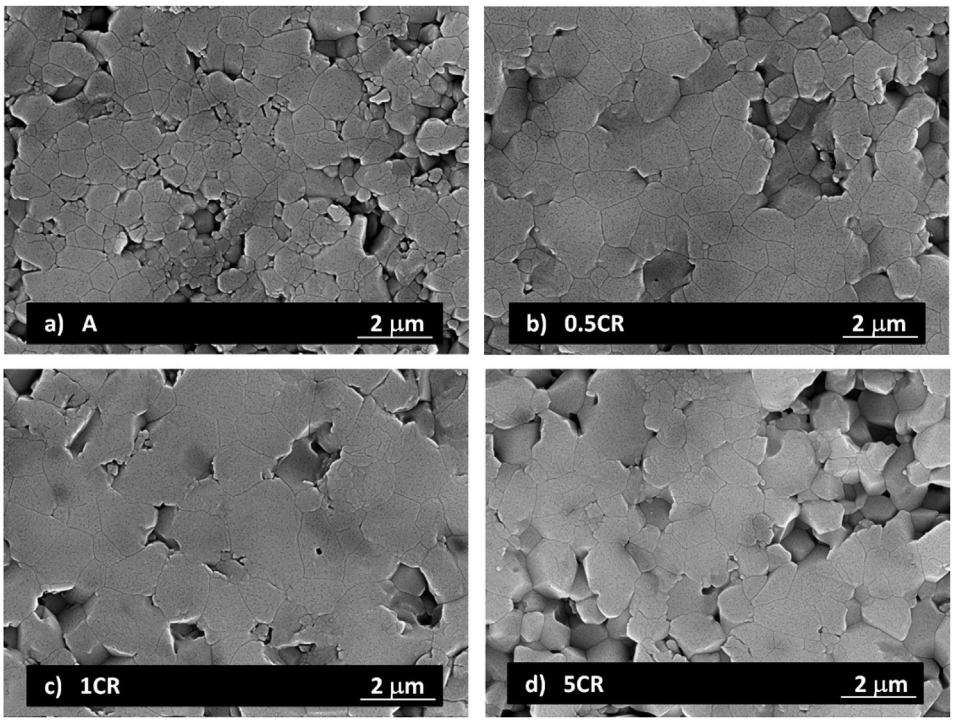

Fig. 2. Thermally etched SEM micrographs of the prepared ceramics a) A, b) 0.5CR, c) 1CR, d) 5CR.

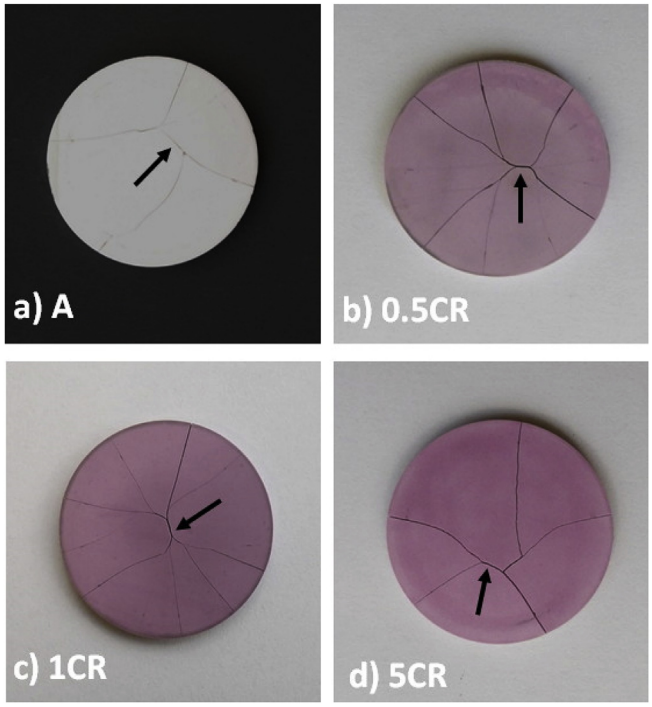

Fig. 3. Disc specimens of all the compositions fractured in the equibiaxial flexural strength test; a) A, b) 0.5CR, c) 1CR, d) 5CR.

(m). The deflection of the cylindrical sample during an equibiaxial flexural strength test can be estimated by using the available solutions for the symmetric bending of circular plates. Deflection of the concentrically loaded simply supported circular plate is given by Timoshenko and at the radius equal to the loading ring radius the deflection can be found by Ref. [32]:

$$\Delta = (w)_{r=b} = \frac{P}{8\pi\delta}\left[(a^2 - b^2)\left(1 + \frac{1}{2}\frac{1-\nu}{1+\nu}\frac{a^2-b^2}{a^2}\right) + 2b^2 log\frac{b}{a}\right] \quad (3)$$

In this equation, w is the deflection of the circular plate (m), a and b are support ring and loading ring radii (m), ν is the Poisson's ratio, and the constant δ is calculated by the following equation:

$$\delta = \frac{Et^3}{12(1-\nu^2)} \quad (4)$$

where E is the elastic modulus (Pa) and t is the thickness of the circular plate (m).

The typical crack patterns for each ceramic without and with different content of Cr_2O_3 additives after the equibiaxial flexural strength tests are presented in Fig. 3. Possible crack initiation sites are shown with arrows on each photograph. The stored elastic energy at fracture increases with the increasing strength of the specimen and at failure release of a larger amount of energy favors the crack front instability and crack branching. The total crack length (hence the total crack surface area) increases with increasing branching. It is observed that Al_2O_3 with low strength has a few branches and a small total crack length. On the other hand, 0.5CR specimens have high strength and many branches (notice that some branches are pale).

The strength of specimens shows a great deal of variation as would be expected from ceramic materials. As a result, total crack surface areas also show a variation. Fig. 4 gives the total crack surface area as a function of the stored elastic energy at fracture and an increasing trend is observed. The solid line on the graph is the linear best fit line for the pooled data set with intercept passing through the origin, i.e. zero crack surface area at zero stored energy. Even though there is considerable scatter, almost all of the 1CR and 5CR data points are located above the best-fit line, indicating a longer crack length for a given stored energy for these compositions. It is possible that the strain energy due to ion size misfit contributes to the stored energy, thus increases the driving energy for crack propagation and slightly increasing the tendency to crack branching in 1CR and 5CR ceramic systems.

Fig. 5 illustrates the fracture surface area of all the ceramics with different Cr_2O_3 contents after the equibiaxial flexural strength test. Levin et al. [33] stated that there are tensile residual stresses in grains and grain boundaries inherently in a sintered pure polycrystalline Al_2O_3 owing to inhomogeneous thermal expansion coefficients and elastic modulus along the crystal axes. The fracture toughness of grain boundaries is lower than within the grains. So, the polycrystalline alumina ceramics have mainly grain boundary fracture (intergranular) mode [34]. In this study, the fracture proceeded mostly by intergranular fracture for the pure Al_2O_3. This crack propagation tendency can also be seen in Fig. 6(a); arrows showing the intergranular crack propagation are dominant. The fracture mode changed from mostly intergranular to a mixture of intergranular and transgranular with Cr_2O_3 addition. As the strength of the pure Al_2O_3 increased by the presence of Cr_2O_3 for all the contents, the mode change was expected because of the localized compressive stresses that induce the strengthening of the grain boundary. The energy required for crack propagation through the grains is higher than the energy needed for crack propagation through the grain boundaries; thus, the fracture mode change indicates the increase in the strength of the material [35,36]. This mixed fracture mode can be seen in Cr-containing compositions both in Fig. 5 and in Fig. 6(b); in Fig. 6(b) arrows for the intergranular and transgranular crack propagation are approximately equal in number indicating a mixed fracture mode.

The average hardness values of the specimens are listed in Table 1. The Al_2O_3–Cr_2O_3 system with 1 vol% Cr_2O_3 content had the maximum Vickers hardness about 22.8 ± 1.3 GPa which means ~13% hardness improvement compared to the pure Al_2O_3. As the content of Cr_2O_3 increased to 5 vol%, the hardness was decreased to 19.0 GPa with the highest standard deviation, ± 2.0. The increase and decrease in hardness values are mainly due to the densification differences in the compositions. Hardness increased with the increase in the relative density but a slight increase (~5.7%) in hardness for 0.5CR ceramics that have the same relative density with the pure Al_2O_3 may indicate the presence of an effect of solid solution formation on the hardness. It was observed that the crack propagation mode changed from intergranular to a mixture of intergranular and transgranular with Cr_2O_3 addition which indicates a grain boundary strengthening generated by Cr^{3+} ions. The grain boundary strengthening may also contribute to the hardening of the ceramic by preventing the microcracking and permanent deformation at the grain boundaries.

Even though crack propagation behavior was intergranular for the pure Al_2O_3 and mixed for the Cr-containing compositions, the fracture toughness values are similar as seen in Table 1. For the pure Al_2O_3, intergranular crack propagation increases the fracture toughness as crack path increases; also grain interlocking and grain pull out contributes to the fracture toughness [37]. On the other hand, for the Cr-containing compositions, ion-misfit strains promoted the strengthening of the interface and forced the crack path to the transgranular mode. When Al_2O_3 grain sizes are smaller than ~2 μm and equiaxed, an improvement in toughness values was observed as fracture mode shifts from intergranular to transgranular [35]. The higher toughness of cleavage fracture compensates for the grain pull–out; thus, the Cr-containing compositions have similar toughness with the pure Al_2O_3.

It is stated that the combination of microstructure, physical properties and the optimization of manufacturing procedure should be considered for choice and evaluation of armour ceramics. For dissipating the kinetic energy of a projectile and preventing the crack propagation, ceramic armour material should satisfy critical property requirements in addition to the related factors including projectile kinetic energy and projectile material properties. Among these properties

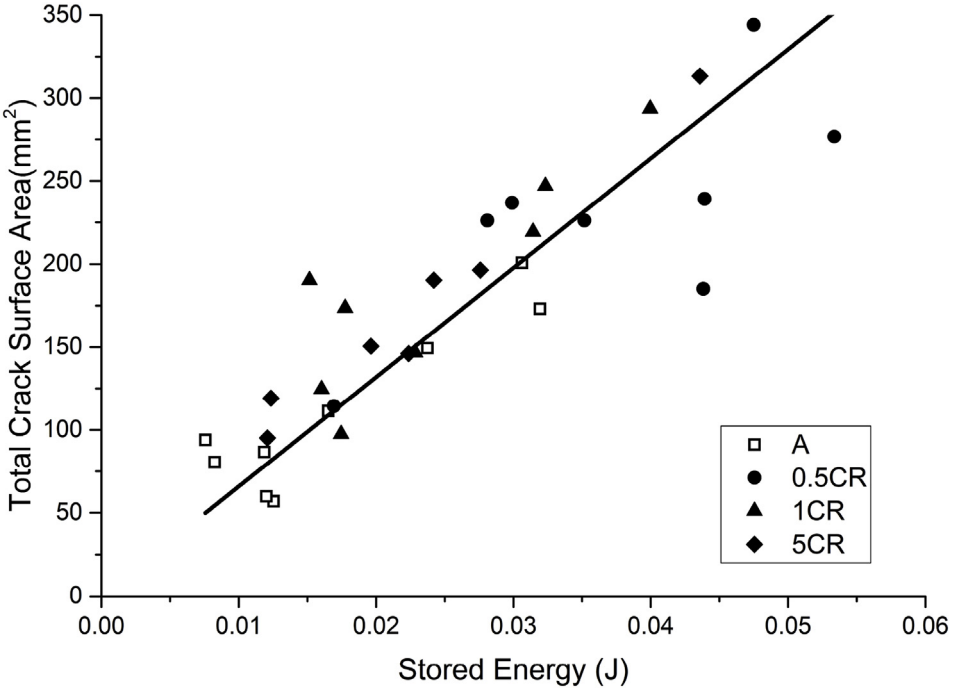

Fig. 4. The total crack surface area as a function of the stored elastic energy at fracture and the best fit line for the pooled data.

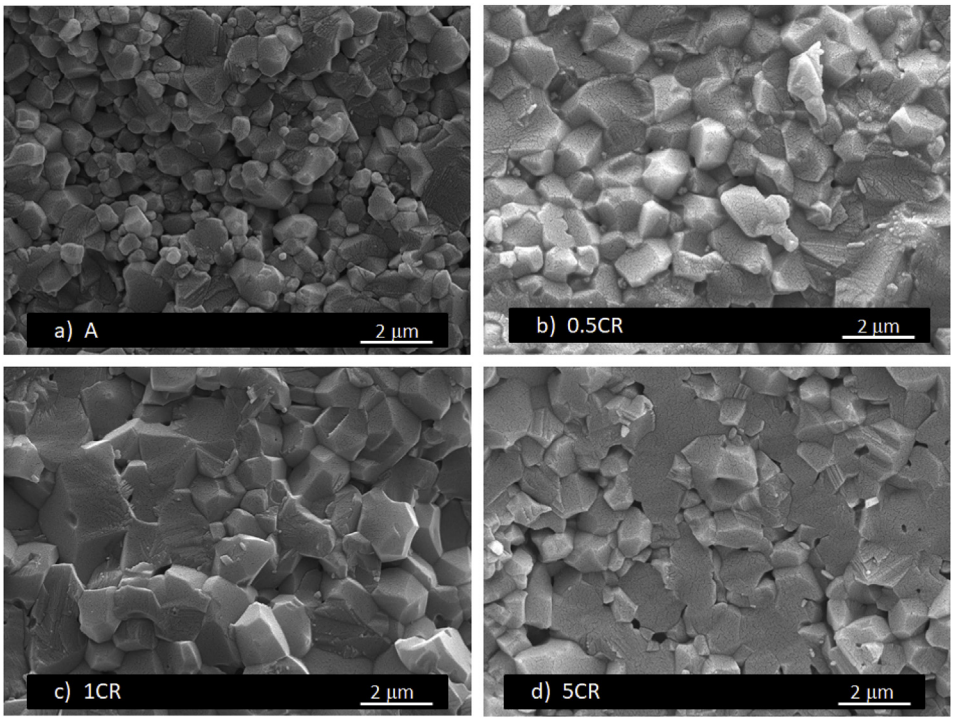

Fig. 5. Fracture surface of the specimens, a) A, b) 0.5CR, c) 1CR, d) 5CR.

density, hardness, fracture toughness, elastic modulus, sonic velocity, and strength are important regarding ceramic armour for the ballistic performance. It is not possible to correlate directly a material property with ballistic performance because the impact of a projectile is a complicated process that crack formation occurs by different factors affecting the stress state in a very short time [38]. High hardness is a very important material property that a ceramic material could deform or fragment the projectile with its high hardness. In addition, abrasive wear interaction of ceramic fragments with the projectile depends on larger and harder fragments of ceramic tile [39]. At constant hardness, a high elastic modulus is important, and a high modulus not only increases the interaction time but also results in a high speed of sound in the ceramic. A higher speed of sound will help a rapid spread of the stress wave and activate a larger region of the ceramic. The hardness has great importance in damaging the projectile in both multi and one-hit conditions. Nevertheless, the fracture from tensile stresses is one of the main failure modes of the ceramic armour and this could not change with the higher hardness of the material. High tensile strength and fracture toughness are required especially under multi-hit conditions to maintain the structural integrity for subsequent hits [40].

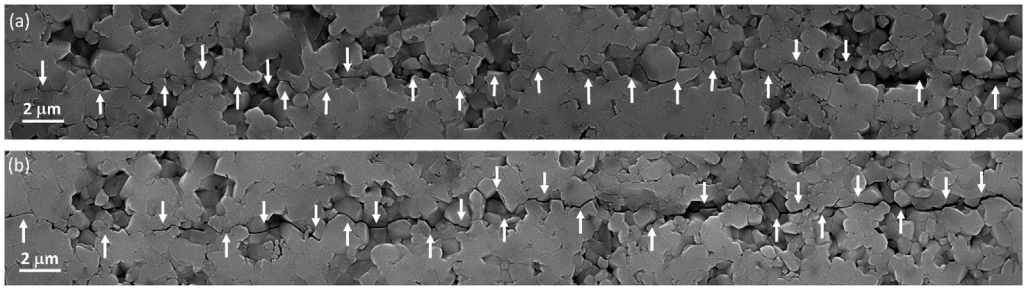

Fig. 6. Propagation characteristic of cracks originating from Vicker's indentation in a) the pure Al_2O_3 and, b) 0.5CR. Downward and upward arrows indicate transgranular and intergranular crack paths, respectively.

For the assessment of the ballistic performance of protective systems, D-criterion was given by Neshpor et al. (in Eq. (5)) that refers the measure of the ability of the ceramic to absorb energy upon impact [18,41].

$$D = \frac{0.36\,(HV \cdot E \cdot c)}{K_{ic}^2} \tag{5}$$

where HV is Vickers hardness, E is elastic modulus, c is sonic velocity (speed of sound in the ceramic) and K_{Ic} is fracture toughness. D-value is valid for one-hit performance of ceramics as a lower value of toughness is required; by contrast, higher toughness values are desired for multi-hits of a ceramic armour component.

In this present study, the addition of Cr_2O_3 on the pure Al_2O_3 provided an increase in hardness and flexural strength of the material without an effect on fracture toughness for 0.5CR and 1CR compositions. The introduced 1CR ceramic system could increase the D-value compared with the pure Al_2O_3 through the obtained high mechanical properties and that may make 1CR system more suitable material for one-hit conditions than Al_2O_3. The total crack surface area-the stored elastic energy correlation shows a shorter crack length for a given stored energy for 0.5CR compared to 1CR, indicating its fragments would be larger in identical impact conditions. Hence, in addition to its highest strength, 0.5CR would increase the erosion of the projectile with larger fragments and may contribute to the performance of the armour under multi-hit conditions.

4. Conclusions

The effect of Cr_2O_3 addition in different volume ratios (0.5, 1, 5 vol %) on microstructure and mechanical properties of Al_2O_3 were examined to assess as an alternative to the pure Al_2O_3 for ceramic armour applications. The microstructure and densification behavior differed with the amount of Cr_2O_3 content and the highest relative density and grain size were obtained for the 1 vol% Cr_2O_3 added ceramic system. Elastic modulus values of ceramics were directly proportional with densification. 0.5 vol% Cr_2O_3 addition increased the flexural strength 44% by the grain boundary modification of the larger size of the Cr^{3+} ions. A 6% and 13% hardness increase was achieved because of the combined effect of increasing relative density and solid solution formation with 0.5 vol% and 1 vol% Cr_2O_3 additions, respectively. Even though the fracture toughness values remained unchanged for all the compositions, the crack propagation behavior turned from mostly intergranular to a mixture of intergranular and transgranular with the Cr_2O_3 addition by the localized compressive stresses that induce the strengthening of the grain boundary. The total crack surface area as a function of the stored energy at failure correlation provided insight into the possible fragmentation behavior of the compositions under ballistic conditions. A shorter crack length for a given stored energy for 0.5 vol% Cr_2O_3 compared to 1 vol%, indicates that its fragments would be larger, and it would increase its abrasive effect during an impact. 0.5 vol% Cr_2O_3 added Cr_2O_3–Al_2O_3 ceramic system with its highest strength could be proposed for multi-hit conditions; while, 1 vol% Cr_2O_3 containing ones may be more suitable for one-hit conditions as higher D-value that could be attained.

Acknowledgment

This work was supported by the Scientific and Technical Research Council of Turkey -TUBITAK through the project no 118M806. Authors also thank Ahmet NAZIM and Adem ŞEN, for their assistance in SEM and XRD analysis of this work, respectively.

Appendix A. Supplementary data

Supplementary data to this article can be found online at https://doi.org/10.1016/j.ceramint.2019.07.037.

References

[1] E. Medvedovski, Alumina–mullite ceramics for structural applications, Ceram. Int. 32 (2006) 369–375 https://doi.org/10.1016/j.ceramint.2005.04.001.
[2] A.Z.A. Azhar, L.C. Choong, H. Mohamed, M.M. Ratnam, Z.A. Ahmad, Effects of Cr_2O_3 addition on the mechanical properties, microstructure and wear performance of zirconia-toughened-alumina (ZTA) cutting inserts, J. Alloy. Comp. 513 (2012) 91–96 https://doi.org/10.1016/j.jallcom.2011.09.092.
[3] J. Jiusti, E.H. Kammer, L. Neckel, N.J. Loh, W. Trindade, A.O. Silva, O.R.K. Montedo, A. De Noni Jr., Ballistic performance of Al_2O_3 mosaic armors with gap-filling materials, Ceram. Int. 43 (2017) 2697–2704 https://doi.org/10.1016/j.ceramint.2016.11.087.
[4] M.V. Silva, D. Stainer, H.A. Al-Qureshi, O.R.K. Montedo, D. Hotza, Alumina-based ceramics for armor application: mechanical characterization and ballistic testing, J. Ceram. (2014) 6. Article ID 618154 https://doi.org/10.1155/2014/618154.
[5] C. Evci, M. Gülgeç, Effective damage mechanisms and performance evaluation of ceramic composite armors subjected to impact loading, J. Compos. Mater. 48 (2014) 3215–3236 https://doi.org/10.1177/0021998313508594.
[6] P. Chabera, A. Boczkowska, A. Morka, P. Kedzierski, T. Niezgoda, A. Ozieblo, A. Witek, Comparison of numerical and experimental study of armour system based on alumina and silicon carbide ceramics, Bull. Pol. Acad.: Tech 63 (2015) 363–367 https://doi.org/10.1515/bpasts-2015-0040.
[7] X. Shi, F. Xu, Z. Zhang, Y. Dong, Y. Tan, L. Wang, J. Yang, Mechanical properties of hot-pressed Al_2O_3/SiC composites, Mater. Sci. Eng. A 527 (2010) 4646–4649 https://doi.org/10.1016/j.msea.2010.03.035.
[8] E.W. Neuman, G.E. Hilmas, W.G. Fahrenholtz, A high strength alumina-silicon carbide boron carbide triplex ceramic, Ceram. Int. 43 (2017) 7958–7962 https://doi.org/10.1016/j.ceramint.2017.03.104.
[9] F. Meng, C. Liu, F. Zhang, Z. Tian, W. Huang, Densification and mechanical properties of fine-grained Al2o3_ZrO2 composites consolidated by spark plasma sintering, J. Alloy. Comp. 512 (2012) 63–67 https://doi.org/10.1016/j.jallcom.2011.09.015.
[10] X.F. Zhang, Y.C. Li, On the comparison of the ballistic performance of 10% zirconia toughened alumina and 95% alumina ceramic target, Mater. Des. 31 (2010) 1945–1952 https://doi.org/10.1016/j.matdes.2009.10.046.
[11] M. Nath, P. Kumar, A.V. Maldhure, S. Sinhamahapatra, K. Dana, A. Ghosh, H.S. Tripathi, Anomalous densification behavior of Al_2O_3–Cr_2O_3 system, Mater. Char. 111 (2016) 8–13 https://doi.org/10.1016/j.matchar.2015.11.005.
[12] M. Nath, S. Sen, K. Banerjee, A. Ghosh, H.S. Tripathi, Densification behavior and properties of alumina–chrome ceramics: effect of TiO_2, Ceram. Int. 39 (2013) 227–232 https://doi.org/10.1016/j.ceramint.2012.06.013.
[13] P. Zhao, H. Zhao, J. Yu, H. Zhang, H. Gao, Qi Chen, Crystal structure and properties of Al_2O_3- Cr_2O_3 solid solutions with different Cr_2O_3 contents, Ceram. Int. 44 (2018) 1356–1361 https://doi.org/10.1016/j.ceramint.2017.08.195.
[14] M. Nath, H.S. Tripathi, Thermo-mechanical behavior of Al_2O_3–Cr_2O_3 refractories: effect of TiO_2, Ceram. Int. 41 (2015) 3109–3115 https://doi.org/10.1016/j.

ceramint.2014.10.155.
[15] C.L. Li, D.H. Riu, T. Sekino, K. Niihara, Fabrication and mechanical properties of Al_2O_3 solid solution with low addition of Cr_2O_3, Key Eng. Mater. 161–163 (1999) 161–164 https://doi.org/10.4028/www.scientific.net/KEM.161-163.161.
[16] D.H. Riu, Y.M. Kong, H.E. Kim, Effect of Cr_2O_3 addition on microstructural evolution and mechanical properties of Al_2O_3, J. Eur. Ceram. Soc. 20 (2000) 1475–1481 https://doi.org/10.1016/S0955-2219(00)00023-6.
[17] M. Kuntz, R. Krüger, The effect of microstructure and chromia content on the properties of zirconia toughened alumina, Ceram. Int. 44 (2018) 211–2020 https://doi.org/10.1016/j.ceramint.2017.10.146.
[18] E. Medvedovski, Ballistic performance of armour ceramics: influence of design and structure. Part 1, Ceram. Int. 36 (2010) 2103–2115 https://doi.org/10.1016/j.ceramint.2010.05.021.
[19] A.A. Wereszczak, J.J. Swab, R.H. Kraft, Effects of Machining on the Uniaxial and Equibiaxial Flexure Strength of CAP3 AD-995 Al_2O_3, U.S. Army Research Laboratory, September 2005 ARL-TR-3617.
[20] A. Healey, J. Cotton, S. Maclachlan, P. Smith, J. Yeomans, Understanding the ballistic event: methodology and initial observations, J. Mater. Sci. 52 (2017) 3074–3085 https://doi.org/10.1007/s10853-016-0594-0.
[21] T. Hirata, K. Akiyama, H. Yamamoto, Sintering behavior of Cr_2O_3-Al_2O_3 ceramics, J. Eur. Ceram. Soc. 20 (2000) 195–199 https://doi.org/10.1016/S0955-2219(99)00161-2.
[22] S.A. Cho, F.J. Arenas, J. Ochoa, Densification and hardness of Al_2O_3–Cr_2O_3 system with and without Ti addition, Ceram. Int. 16 (1990) 301–309 https://doi.org/10.1016/0272-8842(90)90044-G.
[23] H.G. Emblem, T.J. Davies, A. Harabi, A.A. Ogwu, C.S. Nwobodo, V. Tsantzalou, Solid-state chemistry of alumina–chrome refractories, J. Mater. Sci. Lett. 11 (1992) 820–821 https://doi.org/10.1007/BF00730475.
[24] J.F. Xia, H.Q. Nian, W. Liu, X.G. Wang, D.Y. Jiang, Effect of Cr_2O_3 derived from Cr $(NO_3)_3.9H_2O$ precursor on the densification and mechanical properties of zirconia-toughened alumina (ZTA) composites, Ceram. Int. 42 (2016) 9116–9124 https://doi.org/10.1016/j.ceramint.2016.02.176.
[25] D.J. Green, An Introduction to the Mechanical Properties of Ceramics, first ed., Cambridge University Press, 1998.
[26] G.R. Anstis, T. Chantikul, B.R. Lawn, D.B. Marshall, A critical evaluation of indentation techniques for measuring fracture toughness: I, direct crack measurements, J. Am. Ceram. Soc. 64 (1981) 533–538 https://doi.org/10.1111/j.1151-2916.1981.tb10320.x.
[27] X.G. Wang, J.X. Liu, Y.M. Kan, G.J. Zhang, Effect of solid solution formation on densification of hot-pressed ZrC ceramics with MC (M = V, Nb, and Ta) additions, J. Eur. Ceram. Soc. 32 (2012) 1795–1802 https://doi.org/10.1016/j.jeurceramsoc.2011.10.045.
[28] P.R. Bueno, E.R. Leite, L.O.S. Bulhoes, E. Longo, C.O. Paiva-Santos, Sintering, and mass transport features of (Sn, Ti)O_2 polycrystalline ceramics, J. Eur. Ceram. Soc. 23 (2003) 887–896 https://doi.org/10.1016/S0955-2219(02)00234-0.
[29] K. Broniszewski, J. Wozniak, K. Czechowski, L. Jaworska, A. Olszyna, $Al2_O3$_Mo cutting tools for machining hardened stainless steel, Wear 303 (2013) 87–91 https://doi.org/10.1016/j.wear.2013.03.002.
[30] F.H. Lu, H.Y. Chen, C.H. Hung, Degradation of CrN films at high temperature under controlled atmosphere, J. Vac. Sci. Technol. A 21 (2003), https://doi.org/10.1116/1.1566784.
[31] S.C. Han, D.K. Yoon, M.K. Brun, Migration of grain boundaries in alumina induced by chromia addition, Acta Metall. Mater. 43 (1995) 977–984 https://doi.org/10.1016/0956-7151(94)00306-3.
[32] S. Timoshenko, S. Woinowsky-Krieger, Theory of Plates and Shells, second ed., (1959) Singapore.
[33] L. Levin, W. D Kaplan, D.G. Brandon, T. Wieder, Residual stresses in alumina–SiC nanocomposites, Acta Metall. Mater. 42 (1994) 1147–1154 https://doi.org/10.1016/0956-7151(94)90131-7.
[34] H. Awaji, S.M. Choi, E. Yagi, Mechanisms of toughening and strengthening in ceramic-based nanocomposites, Mech. Mater. 34 (2002) 411–422 https://doi.org/10.1016/S0167-6636(02)00129-1.
[35] T. Rodriguez-Suarez a, J.F. Bartolomé, A. Smirnov, S. Lopez-Esteban, R. Torrecillas, J.S. Moya, Sliding wear behaviour of alumina/nickel nanocomposites processed by a conventional sintering route, J. Eur. Ceram. Soc. 31 (2011) 1389–1395 https://doi.org/10.1016/j.jeurceramsoc.2011.02.011.
[36] G.J. Li, X.X. Huang, J.K. Guo, Fabrication and mechanical properties of Al_2O_3-Ni composite from two different powder mixtures, Mater. Sci. Eng. A352 (2003) 23–28 https://doi.org/10.1016/S0921-5093(02)00255-1.
[37] S.W. Freiman, J.J. Mecholsky Jr., The Fracture of Brittle Materials: Testing and Analysis, second ed., John Wiley & Sons, Inc, 2019.
[38] E. Medvedovski, Armor alumina ceramics, in: J.W. McCauley, A. Crowson, W.A. Gooch, Jr.A.M. Rajendran, S.J. Bless, K. Logan, ... S. Wax (Eds.), Ceramic Transactions, vol. 134, Ceramic Armor Materials By Design, The American Ceramic Society, Ohio, 2002, pp. 91–101.
[39] A. Krell, E. Strassburger, Order of influences on the ballistic resistance of armor ceramics and single crystals, Mater. Sci. Eng. A 597 (2014) 422–430 https://doi.org/10.1016/j.msea.2013.12.101.
[40] D.B. Rahbek, B.B. Johnsen, Dynamic Behaviour of Ceramic Armour Systems, Norwegian Defence Research Establishment (FFI), 2015.
[41] V.C. Neshpor, G.P. Zaitsev, E.J. Dovgal, et al., Armour ceramics ballistic efficiency evaluation, in: P. Vincenzini (Ed.), Ceramics: Charting the Future, Proceedings of the 8th CIMTEC, Florence, Italy 28 June–4 July 1994, 1995, pp. 2395–2401.